Composites Science and Technology, Volume 207, May 2021, Article number 108735
DOI: 10.1016/j.compscitech.2021.108735

Effect of Interfacial Fibre Orientation and PPS Veil Density on Delamination Resistance of 5HS Woven CFRP Laminates under Mode II Loading

Amit Ramji[1], Yigeng Xu[1*], Marzio Grasso[1], Mehdi Yasaee[1], Philip Webb[1]

[1] School of Aerospace, Transport and Manufacturing, Cranfield University, Cranfield, MK43 0AL, UK

*Corresponding author: Yigeng.xu@cranfield.ac.uk

Abstract

This paper presents an experimental study on the effect of interfacial fibre orientation and interleaved thermoplastic veil on Mode II interlaminar fracture toughness of 5-harness satin woven carbon fibre reinforced polymer composite laminates. Three-point End-Notched Flexure tests were carried out to determine delamination resistance, G_{IIC} of specimens with five fibre orientation biases and two veil densities at the midplane. Results show that delamination resistance of 5-harness satin woven laminates depends on the layup configurations at the midplane with 90/45 fibre orientation bias exhibiting the greatest resistance. The delamination resistance enhancement from polyphenylene sulfide (PPS) veil interleaves is also fibre orientation dependent but a further increase of the veil density from $10gm^{-2}$ to $20gm^{-2}$ offers little extra benefit. Fracture surface morphologies were examined under SEM to understand the failure mechanism and fracture process of the woven laminate under the combined effects of the interfacial fibre orientation and the veil density. Fibre orientation relative to the delamination path, surface texture misfit, and veil density are the three main contributors identified for the variation of delamination resistance of 5HS woven laminates.

Keywords: Laminate – A; Delamination – B; Fracture toughness – B; Interface – B; Fractography – D

1. Introduction

Laminated composite components have many structural advantages compared with its metallic counterparts. The lack of reinforcement in the thickness direction is however a

major concern for laminated composite components as it facilitates delamination under mode I and mode II loading [1]. Laminated structures are also highly susceptible to out-of-plane impact loading during the manufacturing, operation or maintenance of the structure, which may lead to delamination initiation and significant reductions in their structural performance. Subsequent delamination-induced failure is often associated with local buckling of delaminated plies under combined compression and bending. The complexity of the failure mechanism is exacerbated in woven laminates due to the interlacing and undulating fibre tow microstructures [2]. Woven laminates are also susceptible to membrane-type failures of the sub-laminate due to their lower in-plane strength where interlacing weaves trigger local buckling and bending. Delamination tendencies can arise from local features such as voids and resin-rich regions. These constraints typically lead to excessively over-conservative designs with multiple load paths. Toughening of laminae interfacial regions could however provide a viable solution.

Research efforts to improve the Interlaminar Fracture Toughness (ILFT) and delamination resistance by modifying the material constituents have demonstrated significant progress over the years. Modifications to matrix chemistry, fibre surface treatments, commingling with tougher fibres, interleaving [3–13] and through-thickness reinforcements have all presented improvements in ILFT, delamination growth resistance and damage tolerance capacity. Toughening methods using thermoplastic interleaves can allow exploitation of the tough and ductile interleave layer, which improves the ILFT in mode I and mode II, namely, G_{IC} and G_{IIC} [5,8,11,14–19]. The potential to incorporate toughening at bespoke interfaces and locations with little extra cost is an added benefit only possible with interleaving in comparison to the other modification techniques mentioned above.

The increasing use of 5-harness satin (5HS) carbon fibre reinforced polymer (CFRP) laminates are due to the two-dimensional weave improving pliability hence draping quality in comparison to Unidirectional, Twill or Plain weave. Formability on curved contours

increases and results in a smooth and seamless appearances as the number of the satin weave fibres increases, however fabric stability can decrease beyond the 5HS weave. While delamination remains an important failure attribute, few studies [7,20–23] have considered the effect of stacking sequence of 5HS woven laminates on delamination resistance in detail. There is no publication in open literature investigating the influence of polyphenylene sulfide (PPS) interleaves on the fracture toughness of 5HS woven composites combined with various interfacial fibre orientation biases at the midplane. The motivation of this work aims to fill the gap by presenting a systematic experimental study to understand the combined effect of the interfacial fibre orientation bias and PPS veils on the mode II ILFT (G_{IIC}) of 5HS CFRP laminates.

2. Materials and Experimental Procedures

Pre-impregnated 5HS CFRP supplied by Cytec was selected for the 3-point end-notched flexure (3ENF) tests, consisting of 5HS woven carbon 3K Toray T1000 fibres and MTM49 toughened epoxy [24] of 42% resin weight. The 5HS CFRP material has an areal density of 283gm^{-2}, a nominal ply cure thickness of 0.35mm and mechanical properties in Table 1.

Table 1 Mechanical properties of *MTM49-3-42%-3KFT300B40B-5H-283-1000* [24].

Mechanical Properties	**Results**
0° Tensile strength (MPa)	1065
0° Tensile modulus (GPa)	44.6
90° Tensile strength (MPa)	1035
90° Tensile modulus (GPa)	42.8
0° Compressive strength (MPa)	640
0° Compressive modulus (GPa)	59
90° Compressive strength (MPa)	610
90° Compressive modulus (GPa)	57
In-plane shear strength (MPa)	108
In-plane shear modulus (GPa)	2.5
0° Interlaminar shear strength (MPa)	64.2

Orientation balanced outer plies of the 5HS woven laminates were prepared around a central layer of nonwoven PPS veil with two density variants for comparison against a non-interleaved control group with the same layup configuration. The PPS veil supplied by Technical Fibre Products is Optiveil OP-49-48 [25], with an areal density of 10gm^{-2} and

thickness of 0.09mm. The veils were manufactured using a wet-lay process with chopped strand PPS fibres of 10μm diameter and 6mm in length within a styrene-acrylic binder. The 5HS fabrics (Fig.1) show weft yarns pass over four warp yarn tows and under one, allowing for improved pliability compared with plain or twill weave fabrics. The in-plane mechanical properties of 5HS fabrics have negligible strength and stiffness differences between the warp and weft directions as the reinforcement fibre count is balanced (Table 1), Unlike plain or twill weave, 5HS weave architectures have an inherent in-plane fibre orientation bias exhibiting different dominant fibre orientations at its top and bottom faces, which may affect the mechanical performance of laminates with different layup configurations [18]. Fig.1(a) illustrates the fibre orientation bias in the warp and weft directions for each face when considering a segment of the 5HS fabric: Face A is dominated by (4:5 or 80%) 0° fibre orientations while Face B is dominated by (4:5 or 80%) 90° fibre orientations. Fig.1(b) provides a visual representation of an example layup with 90/90 fibre orientation bias at the midplane.

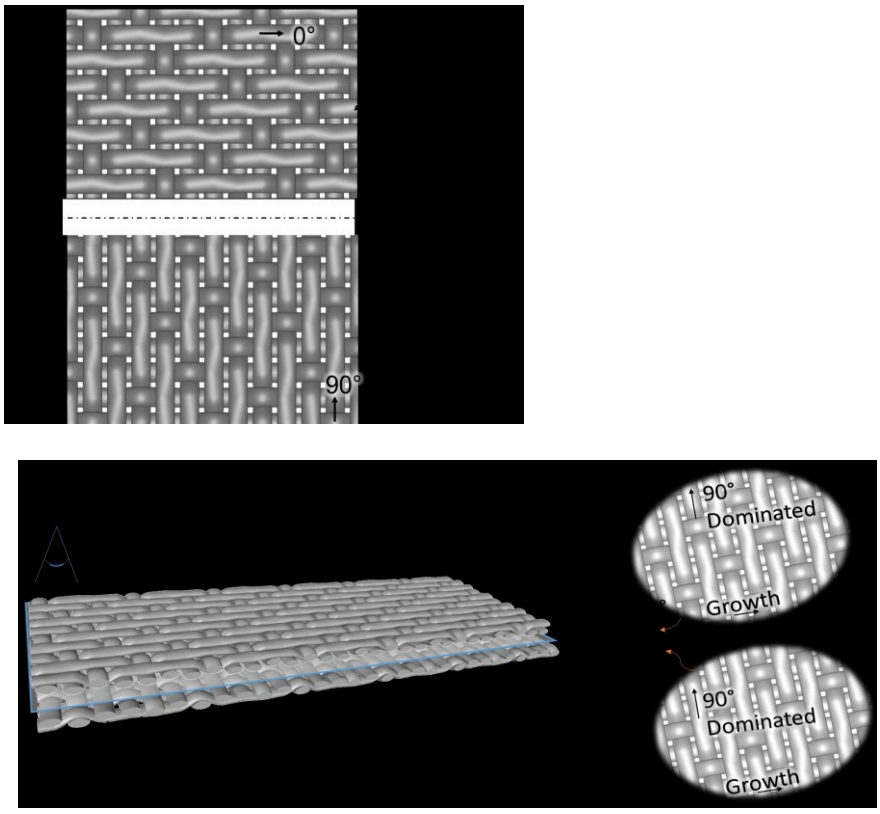

Fig.1 (a) Fibre architecture and orientation bias at each 5HS CFRP face and
(b) Layup example for 90/90 fibre orientation biased midplane.

The layup configurations of the 3ENF specimens with the dominant midplane fibre orientations being 0/0, 0/45, 0/90, 90/45 and 90/90 are listed in Table 2. By introducing two veil densities ($10gm^{-2}$, $20gm^{-2}$) along with a control midplane, fifteen sample configurations were investigated in three groups. The first group of five sample configurations contains no interleaves and is the control group for the comparative study for the effect of PPS veil on ILFT. The second group of five configurations contains a single layer of PPS veil of areal density $10gm^{-2}$ interleaved at the midplane adjacent to the 5μm PTFE release film used for forming the initial crack. The third group of five configurations contained two layers of veils interleaved at the midplane to build the veil areal density up to $20gm^{-2}$.

Table 2 Layup configuration, midplane fibre orientation bias, and configuration code.

Layup Configuration (Viewed from top)	**Midplane Fibre Orientation Bias**	**Configuration Code**
$[0,90]_6$	0/0	0/0
$[(0,90)_3$, 1 veil, $(0,90)_3]$		10v-0/0
$[(0,90)_3$, 2 veils, $(0,90)_3]$		20v-0/0
$[90_6,-45,90_5]$	0/45	0/45
$[90_6$, 1 veil, $-45,90_5]$		10v-0/45
$[90_6$, 2 veils, $-45,90_5]$		20v-0/45
$[0,90]_{3s}$	0/90	0/90
$[(0,90)_3$, 1 veil, $(90,0)_3]$		10v-0/90
$[(0,90)_3$, 2 veils, $(90,0)_3]$		20v-0/90
$[0_6,-45,0_5]$	90/45	90/45
$[0_6$, 1 veil, $-45,0_5]$		10v-90/45
$[0_6$, 2 veils, $-45,0_5]$		20v-90/45
$[90,0]_6$	90/90	90/90
$[(90,0)_3$, 1 veil, $(90,0)_3]$		10v-90/90
$[(90,0)_3$, 2 veils, $(90,0)_3]$		20v-90/90

Test standard ASTM D7905-14 [26] intended for G_{IIC} measurement of unidirectional (UD) composite laminates with a 0°/0° midplane was adopted for the current study owing to no standard available for the G_{IIC} measurement of woven laminae composites. The stacking configuration deviates slightly from the standard symmetric layup configuration $[0_n]_s$ specified in ASTM D7905-14. This is inevitable as this study focuses on the effect of interfacial fibre orientation and interleaved veil on ILFT, which cannot be achieved with the biased interfaces of 5HS weaved plies. Fig.2(a) illustrates the 3ENF specimens with the

nominal dimensions of 180mm in length, 20mm in width and 4mm in thickness. Twelve 5HS weaved CF/Epoxy layers were de-bulked under vacuum and subsequently placed on a flat steel plate with peel film, caul plate, breather fabric and cured inside a vacuum bag within the autoclave. The panels were cured under pressure at 0.62 MPa, with a target bag vacuum of <0.005MPa, ramp rates of 3°C/min and a dwell temperature of 135°C for 90 minutes as prescribed for MTM49 [24]. Following the curing and debagging, individual repeat specimens were cut and numbered from a single plate using a water-flooded diamond saw.

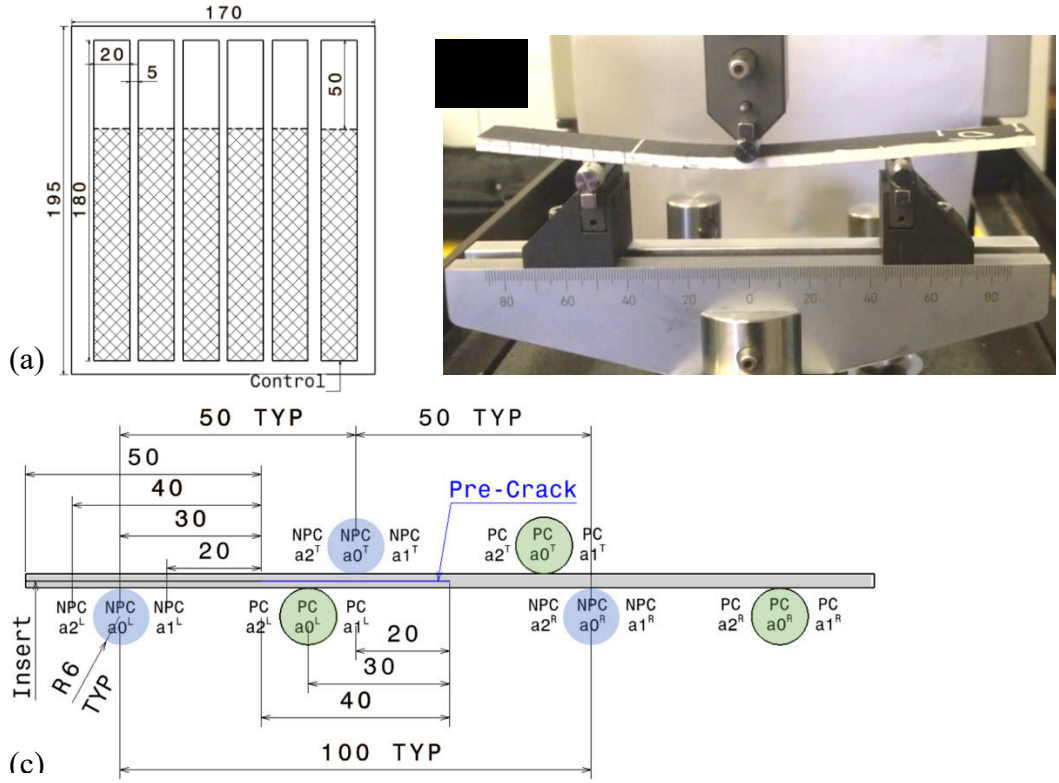

Fig.2 (a) Laminate plate geometry, (b) setup for 3ENF test, (c) 3ENF loading positions

To enhance contrast, the specimen edges were sprayed with a thin film of white paint to aid tracking of the delamination for specimen positioning (Fig 2(b)). An ultrasonic scanner was used to compare and verify the crack position visible on the specimen edges. A Sonatest Veo 16:64 with a 64 linear element probe in a submerged water tank was used before each compliance and fracture test for the detailed identification of delamination using the PTFE insert edge as a datum (Fig.2(c)). The achieved delamination front was also scanned after

each test to mark the delamination for subsequent pre-cracked compliance and fracture tests. The 3ENF testing was conducted on a dual-screw column servo-electric universal test machine (Instron 5965), equipped with a calibrated 5kN load cell. The crosshead displacement rate was set to 0.5mm/min to maintain quasi-static loading conditions and allow tracking of the delamination growth. The tests were also recorded using a 150mm macro lens and tripod-mounted DSLR camera at 60 frames/second for subsequent examination of the delamination process.

For each sample configuration, three repetitions were carried out following ASTM-D7905/M–14 [26] to obtain an average G_{IIC} value. During each test, the specimens were positioned in a 3-point bending fixture (Fig.2(b)) with Ø=12mm steel rollers. The end-notched flexural tests were conducted at six positions illustrated in Fig.2(c) which provided the required information for Non-Pre-Cracked (NPC) and Pre-Cracked (PC) compliance calibration and fracture test results for each specimen. Firstly, compliance calibration (CC) tests were performed by loading the specimens to the peak CC force equal to 50% of the expected value of the critical force and then unloading. The compliance calibration test specimens were positioned so that the left roller was 20mm (a_1) and 40mm (a_2) behind the crack tip (Fig.2(c)). Secondly, the G_{IIC} values for delamination initiation and growth were obtained when the left roller was positioned at 30mm from the insert (NPC) and the pre-crack (PC) at the a_0 loading positions. For fracture tests ($NPCa_0$ and PCa_0), the specimens were loaded until the delamination advance was observed visually on the sprayed edge and by the stiffness reduction on the force-displacement plot (indicators on Fig.3). The subsequent unloading was carried out at 0.5 mm/min, with force and displacement data recorded continuously at a sampling rate of 5 Hz. The use of the same specimen for fracture tests has been demonstrated to produce accurate NPC and PC toughness values [26] and is followed within this study. For ILFT calculations, the two CC coefficients from each NPC and PC tests were determined prior to the fracture tests (a_0). Initiation values of G_{IIC} were

obtained from the maximum force (P). The CC coefficients, A and m, were determined using a least-square linear regression analysis of the compliance, C, versus crack length cubed (a^3):

$$C = A + ma^3 \quad (1)$$

where A is the intercept and m is the slope obtained from the regression analysis.

The mode II strain energy release rate, G_{II}, was determined with the compliance calibration (CC) relation specified in ASTM-D7905/M–14 [26] for specimens with constant width, B:

$$G_{II} = \frac{P^2}{2B}\frac{\partial C}{\partial a} \quad (2)$$

Substituting the compliance in Eq.(1) into Eq.(2) and taking the partial derivative leads to:

$$G_Q = \frac{3mP^2a^2}{2B} \quad (3)$$

The mode II $NPCa_0$ and PCa_0 candidate fracture toughness (G_Q) was determined using Eq.(3), where P is the maximum load from the fracture test (a_0) and a is the initial crack length. The candidate toughness (G_Q) was determined and checked for validity as specified in ASTM D7905/M–14 [26] to be inferred as G_{IIC}.

Validity is determined if $15\% \leq \%G_Q \leq 35\%$, where

$$\%G_{Qj} = \left[\frac{100(P_j a_j)^2}{(Pa_0)^2}\right]; \quad j = 1, 2 \quad (4)$$

The $\%G_{Qj}$ are the two values of G_Q associated with the compliance tests at a_1=*20mm* and a_2=*40mm* respectively. P_{a0} is the maximum load from the initiation of non-linearity illustrated in Fig.3 for the fracture tests carried out when a_0=30mm.

3. Results - Effect of interfacial fibre orientation and veil on load-displacement behaviour

Fig.3 presents the representative load-displacement curves of the 3ENF tests for specimens with various interfacial fibre orientation. The arrows indicate the end of the linearity region of the load-displacement, which are used to determine the maximum load P_{a0} in Eq.(3).

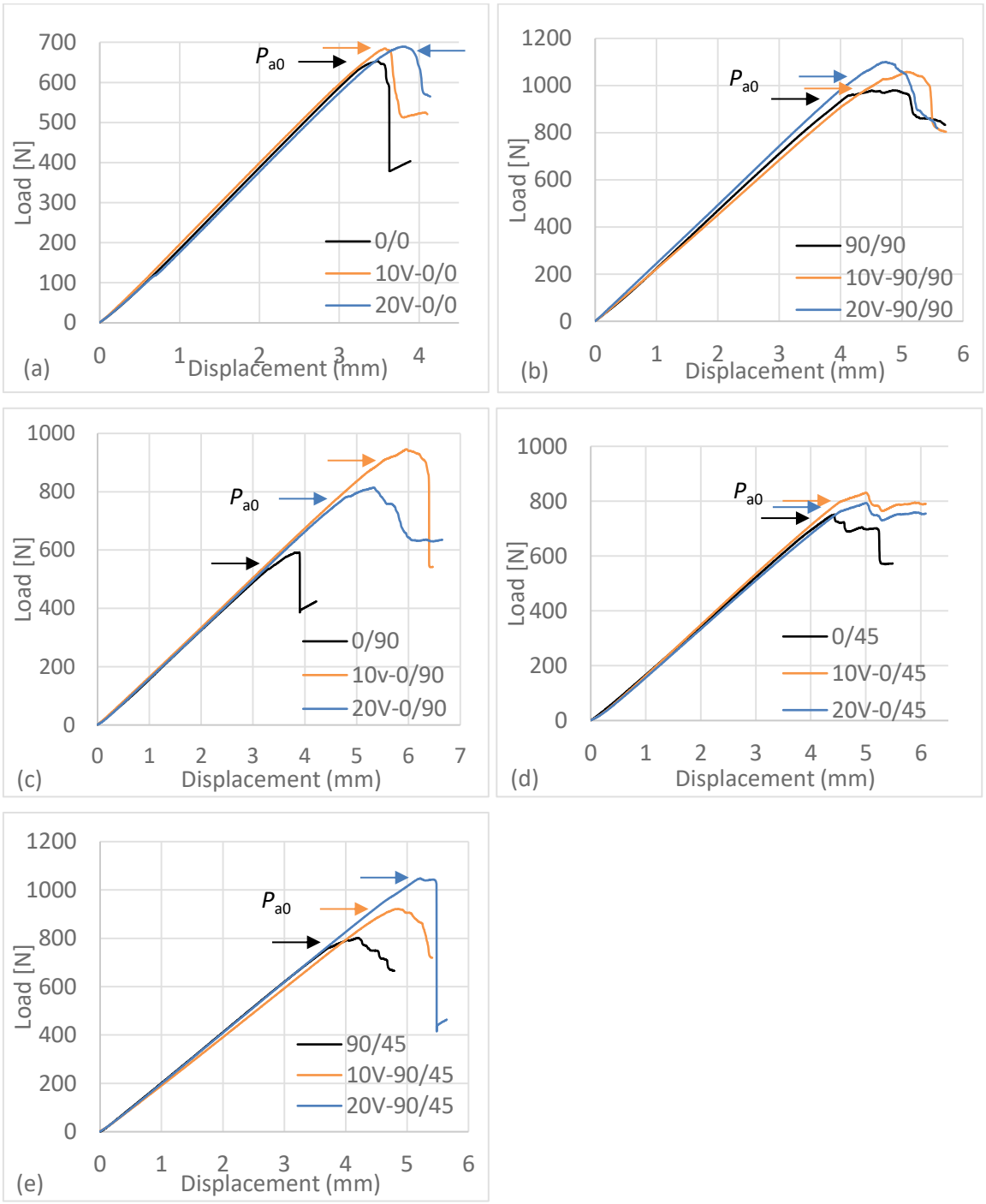

Fig.3 Representative load-displacement for PCa_0 test: (a) 0°/0°, (b) 90°/90°, (c) 0°/90°, (d) 0°/45° and (e) 90°/45° biased midplanes.
Note: Markers indicate P_{a0} = Pre-crack peak force (end of linear-elastic region).

The enclosed area under each load-displacement curve represents the delamination resistance, hence closely related to the ILFT in mode II. It can be observed in Fig.3(a-e) that the interfacial fibre orientation and the addition of interleaved veils affect the peak force of the load-displacement curve and hence the enclosed area. The veil interleaved configurations have greater peak loads and displacements than the non-interleaved

configurations. The load-displacement curves of the 0/0 midplane fibre orientation exhibit a sudden reduction of the load after the peak force as presented in Fig.3(a), which is linked to a sudden delamination growth during the loading process, particularly for configurations without the veil. Other configurations such as the 90/90 midplane fibre orientation bias (Fig.3(b)) have a greater slope of the load-displacement curve and a gradual load reduction during fracture compared with the 0/0 midplane fibre orientation bias (Fig.3(a)). This indicates that specimens with non-0/0 midplane fibre orientation bias have greater load carrying capacity and the fracture process is more stable.

A range of peak forces were observed during the fracture tests for configurations with different interfacial fibre orientations and veil densities. The variations in maximum load are associated with varying interfacial fibre-matrix interactions under mode II loading. These variations are associated with diverse energy dissipation mechanisms during the fracture process, hence have different delamination resistances for the interfacial fibre orientations and veil density configurations. The effect of veil on the G_{IIC} is heavily dependent on the interfacial fibre orientation based on the observations in this work, and is consistent to the authors' previous work on UD materials [18]. Fracture surface morphologies were examined under SEM in Section 4 to understand the failure mechanism and fracture process of the woven laminate under the combined effect of interfacial fibre orientation bias and interleaved PPS veil.

Table 3 summarizes the mean values and standard deviations of G_{IIC} for the fifteen layup configurations separating into the three interleaving categories (supplementary data and sample calculation in appendix). Significant variations in G_{IIC} for interfaces with different fibre orientation biases can be observed. The PPS veils not only improve the fracture resistance but also reduce the scattering of the test data when the veil density has reached $20gm^{-2}$. The reduced scatter can be linked to the more stable delamination process when the veil density is increased to toughen the midplane.

Table 3 Summary of 3ENF test results.

Midplane fibre orientation bias	G_{IIC} (veil density: 0) [J/m^2]		G_{IIC} (veil density: 10gm^{-2} veil) [J/m^2]		G_{IIC} (veil density: 20gm^{-2} veil) [J/m^2]	
	Mean	StdDev	Mean	StdDev	Mean	StdDev
0/0	1055	84	1607	96	1630	49
0/45	1811	181	2255	80	2228	143
0/90	1007	35	1723	64	1760	11
90/45	1921	196	2327	172	2377	99
90/90	1858	131	2364	119	2375	38

Results in Table 3 are plotted in Fig.4 to highlight the effect of interfacial fibre orientation and interleaved veil density of delamination resistance. Fig.4(a) focuses on the effect of interfacial fibre orientation on delamination resistance where the G_{IIC} variations with layup configurations are grouped under veil densities of 0gm^{-2}, 10gm^{-2}, and 20gm^{-2}, respectively. The percentage variation of G_{IIC} in Fig.4(a) is calculated against the G_{IIC} value of the specimens with 0/0 interfacial fibre orientation bias without veil at the midplane. It can be observed that all three groups of G_{IIC} data in Fig.4(a) follow the same pattern of variations with interfacial fibre orientation biases. Regardless of the veil density, configurations with 45° midplane fibre orientation bias (i.e. 0/45 and 90/45) exhibit the strongest delamination resistance with both 20v-0/45 (2375J/m^2) and 20v-90/45 (2377J/m^2) having G_{IIC} 125% greater than the 0/0 configuration (1055J/m^2).

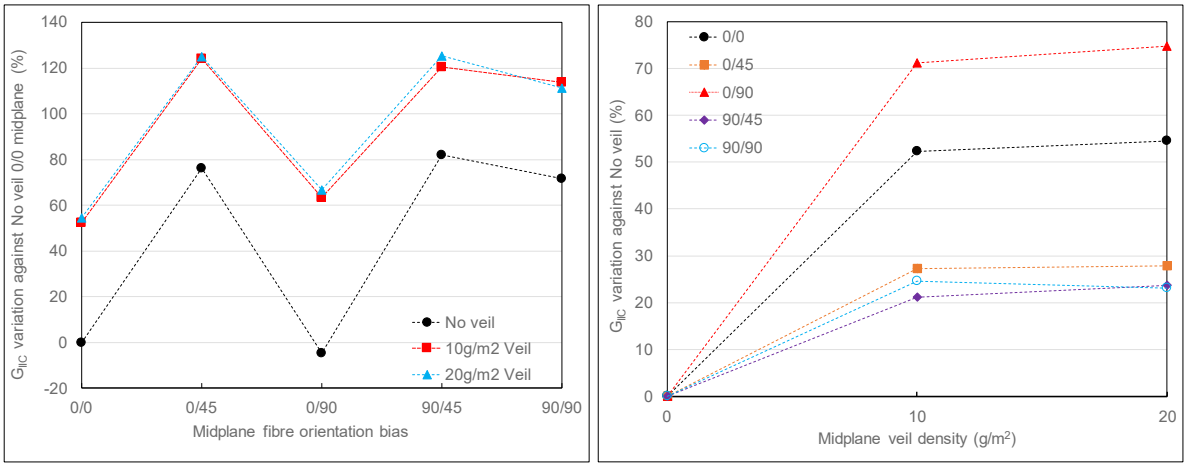

(a) (b)

Fig.4 Variations of G_{IIC} due to (a) interfacial fibre orientation and (b) veil density.

Fig.4(b) focuses on the effect of veil densities on delamination resistance where the G_{IIC} variations are presented for each midplane fibre orientation bias. The percentage variation of G_{IIC} in Fig.4(b) is calculated against the G_{IIC} value of the non-interleaved group with the same interfacial fibre orientation bias. It can be observed that introduction of the PPS veil to the midplane improves the delamination resistance of the 5HS woven laminates for all five interfacial fibre orientation biases investigated. The G_{IIC} improvement from the veil is however dependent on the interfacial fibre configuration with the 0/90 interfacial fibre orientation bias exhibiting the greatest improvement. Compared with the non-interleaved 0/90 configuration (1007J/m2), 10v-0/90 (1723J/m^2) and 20v-0/90 (1760J/m^2) specimens exhibit enhancements of 71% and 75% in G_{IIC}. It is also worth noting that a further increase of veil density from 10gm^{-2} to 20gm^{-2} offers little [8] extra enhancement in G_{IIC} for all five interfacial fibre orientation biases investigated.

4. Results - Fracture morphology at interfaces of varying fibre orientation and veil density

To understand the effect of interfacial fibre orientation and veil density on delamination resistance of 5HS woven laminate, fracture surface morphologies were examined under Scanning Electron Microscopy (SEM): a Zeiss Evo 50 Digiscan II with a 15kV beam and emitter distance between 6.5mm to 9mm. While intra-laminar fracture and global delamination migration [18] are not possible in 5HS laminates due to the weave architecture, the fractographic features including surface texture, fibre bridging and breakage, resin-rich pockets, and other contributing factors can rationalise variations of G_{IIC} with interfacial fibre orientation and veil density as shown in Table 3 and Fig.4.

Fig.5 presents the SEM observations of the fracture surface of 0° fibre orientation bias at the midplane with dominant 0/0 fibre orientations. Interleaved configurations (Figs.5(b-c)) exhibit a coarser and irregular surface texture than the non-interleaved configuration (Fig.5(a)), owing to the effect of veil density on delamination resistance. The pronounced

presence of broken fibres tows, resin remnants and surface striations of interleaved groups indicate increased fibre-matrix interactions and energy dissipation during the fracture process, demonstrating that veil interleaving had a significant influence on the delamination resistance. The enhanced surface roughness and fibre-matrix interactions can explain the G_{IIC} improvements of 52% for 10v-0/0 (1607J/m^2) and 55% for 20v-0/0 (1630J/m^2) configurations against the non-interleaved 0/0 (1055J/m^2) (Table 3 and Fig.4). The observations are consistent with those observed for thermoplastic veil interleaves on fracture toughness enhancements of UD laminates [4,5,11,12,18].

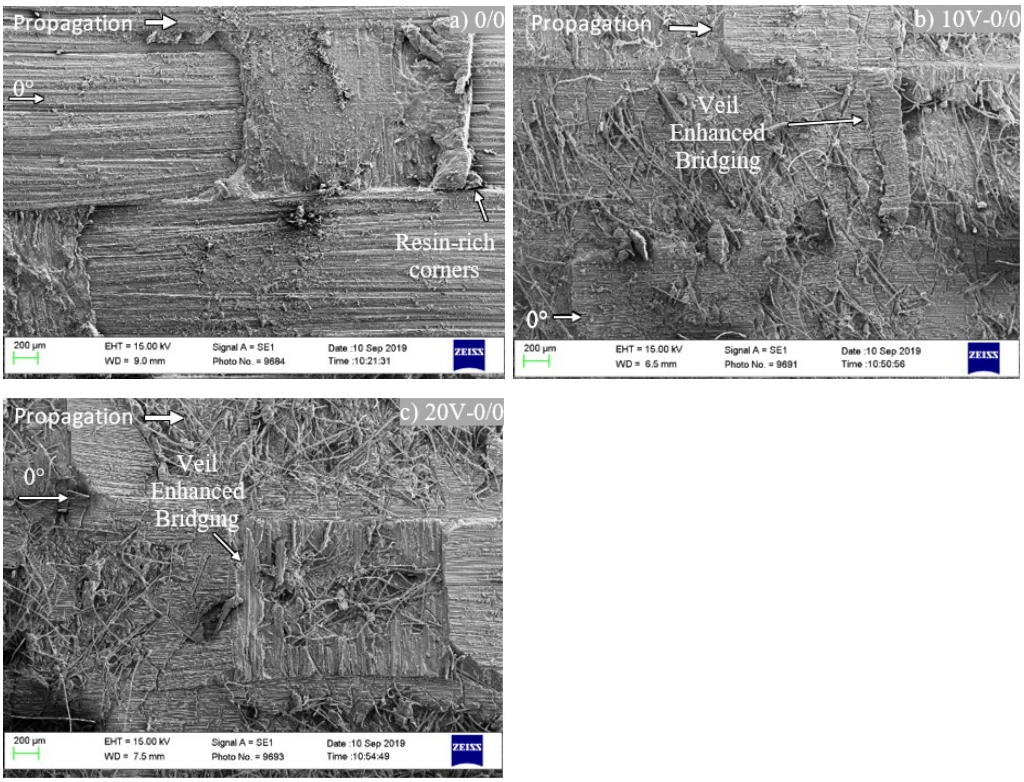

Fig.5 Fracture surface of 0° fibre orientation bias at 0/0 dominated midplane: (a) without veil, (b) 10gm^{-2} veil, and (c) 20gm^{-2} veil.

Fig.6 presents the SEM observations of the fracture surface of 45° fibre orientation bias with dominant 0/45 midplane fibre orientation at the midplane. Compared to the non-interleaved 0/0 dominant fibre orientation (Fig.5(a)), configurations with dominant 0/45 midplanes (Fig.6(a)) exhibits traces of 0° fibre imprints. Additionally, interleaved configurations (Figs.6 (b-c)) contain tow-localised tendencies for mixed-mode II/III fracture and cusp features triggered by the off-axis 45° dominated ply. The nonuniform delamination front introduces

greater delamination resistance, hence justifies a 76% increase in G_{IIC} of the non-interleaved 0/45 (1858J/m^2) midplane compared with the non-interleaved 0/0 (1055J/m^2) (Table 3 and Fig.4). The interleaved 0/45 configuration (Figs.6(b-c)) exhibit significant surface irregularities, fibre breakages, fibre-resin imprints and shear hackles due to local shear stresses compared with the non-interleaved group (Fig.6(a)). The resulting G_{IIC} improvements of 27% for 10v-0/45 (2364J/m^2) and 28% for 20v-0/45 (2375J/m^2) can be achieved over the non-interleaved 0/45 (1858/m^2) specimens. The combined effect of interfacial fibre orientation bias and interleaved PPS veils makes the G_{IIC} of 10v-0/45 and 20v-0/45 specimens 124% and 125% higher than that of the non-interleaved 0/0 specimens.

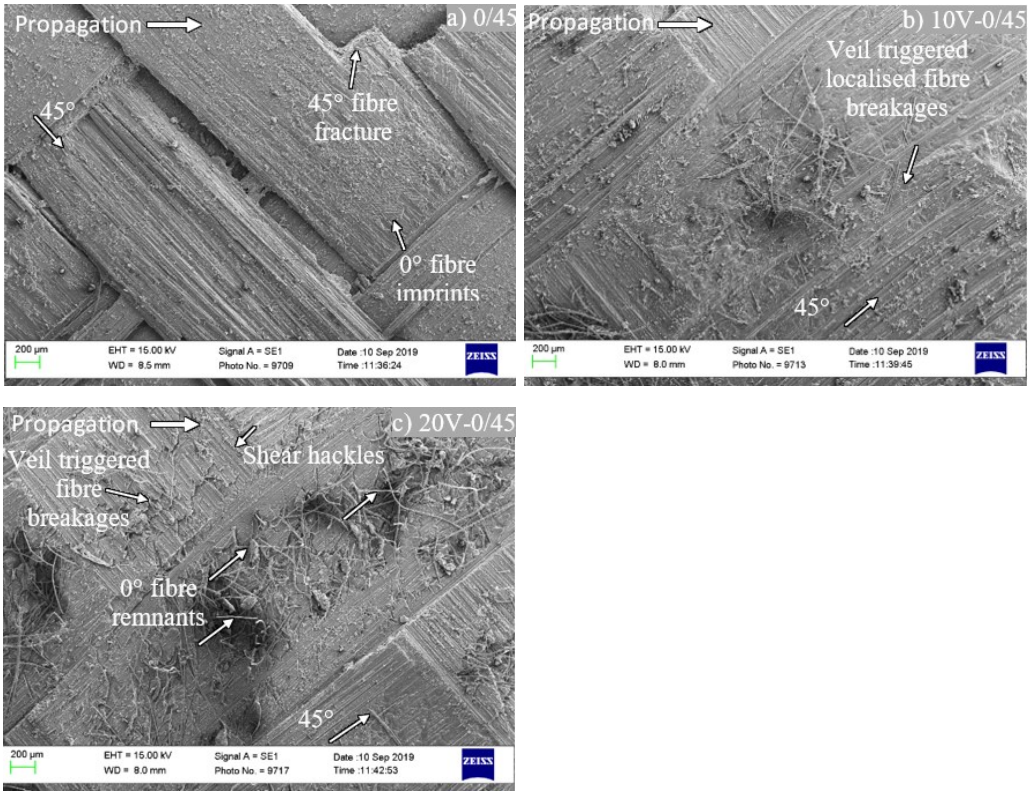

Fig.6 Fracture surface of 45° fibre orientation bias at 0/45 dominated midplane: (a) without veil, (b) 10gm^{-2} veil, and (c) 20gm^{-2} veil.

Fig.7 presents the SEM observations of the fracture surface of 0° fibre orientation bias at the midplane with dominant 0/90 interfacial fibre orientation. Compared to the non-interleaved 0/0 dominant midplane (Fig.5(a)), non-interleaved 0/90 dominant midplanes (Fig.7(a)) present similar fracture surface features except that the fracture surface in Fig.7(a) have increased resin rich regions than in Fig.5(a). The 90° misfit between the faces

of the 0° and 90° fibre orientation bias may facilitate the formation of the resin rich zone in the non-interleaved 0/90 configuration. The weakening effect of the resin rich zones on G_{IIC} may offset the toughening effect of the 90° fibres perpendicular to the delamination propagation direction, explaining the 5% decrease in G_{IIC} of the non-interleaved 0/90 (1007J/m^2) compared with the non-interleaved 0/0 (1055J/m^2) specimens (Table 3 and Fig.4). The interleaved 0/90 specimens (Figs.7(b-c)) exhibit a coarser fracture surface than the non-interleaved group (Fig.7(a)) with localised fibre peeling, breakages and fewer resin rich zones due to the resin absorption of the veil interlayer. The resulting features explain the G_{IIC} improvements of 71% for 10v-0/90 (1723J/m^2) and 75% for 20v-0/90 (1760J/m^2) over the non-interleaved 0/90 (1007/m^2) specimens. The combined effect of interfacial fibre orientation bias and the PPS veil makes the G_{IIC} of 10v-0/90 and 20v-0/90 specimens 63% and 67% greater than the non-interleaved 0/0 configuration.

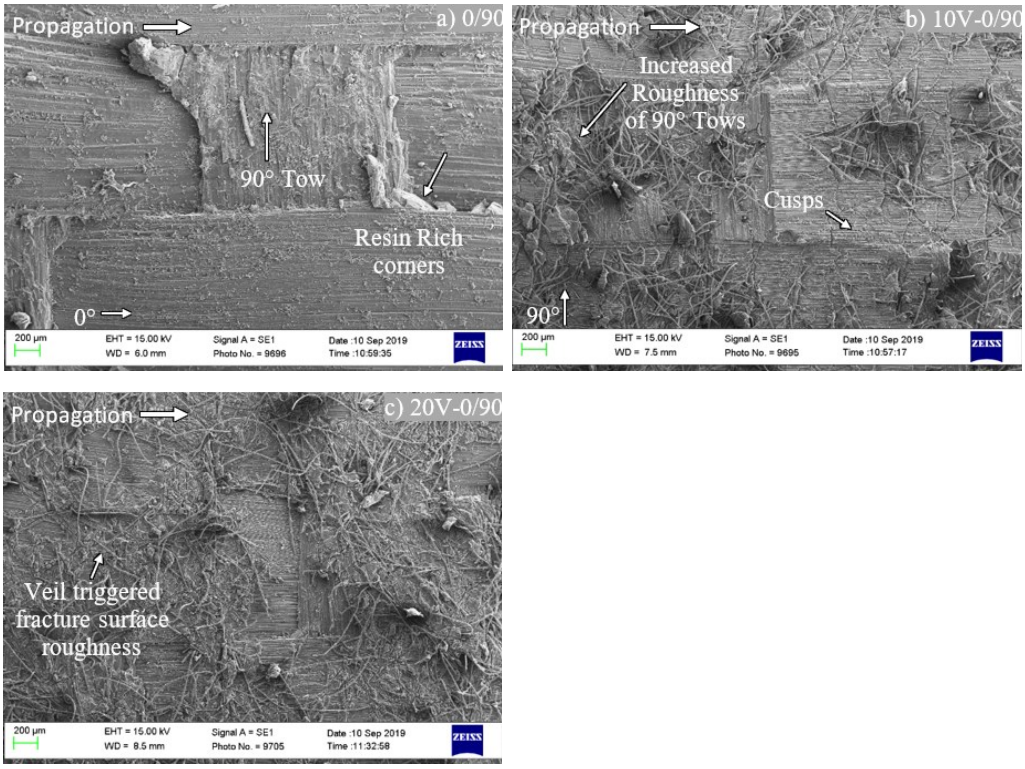

Fig.7 Fracture surface of 0° fibre orientation bias at 0/90 dominated midplane: (a) without veil, (b) 10gm^{-2} veil, and (c) 20gm^{-2} veil.

Fig.8 presents the SEM observations of the fracture surface of the 45° fibre orientation bias at the midplane with a dominant 90/45 midplane fibre orientation. Compared to the

interleaved 0/0 midplane fibre orientation (Figs.5(b-c)), interleaved 90/45 midplanes (Figs.8(b-c)) present evidence of tow-localised tendencies for mixed-mode II/III features triggered by the off-axis 45° dominated ply. Both the nonuniform delamination front and the transverse fibres of the 90° fibre orientation bias contribute to the increased delamination resistance, explaining the 82% increase in G_{IIC} for the non-interleaved 90/45 (1921J/m^2) compared with the non-interleaved 0/0 (1055J/m^2) specimens (Table 3 and Fig.4). The interleaved 90/45 specimens (Figs.8(b-c)) exhibit greater surface irregularity with fibre pull out and fractures compared to the non-interleaved (Fig.8(a)), explaining the G_{IIC} improvements of 21% for 10v-90/45 (2327J/m^2) and 24% for 20v-90/45 (2377J/m^2) over the non-interleaved 90/45 (1921/m^2) specimens. The combined effect of interfacial fibre orientation bias and the PPS veil makes the G_{IIC} of 10v-90/45 and 20v-90/45 specimens 121% and 125% greater than the non-interleaved 0/0 configurations.

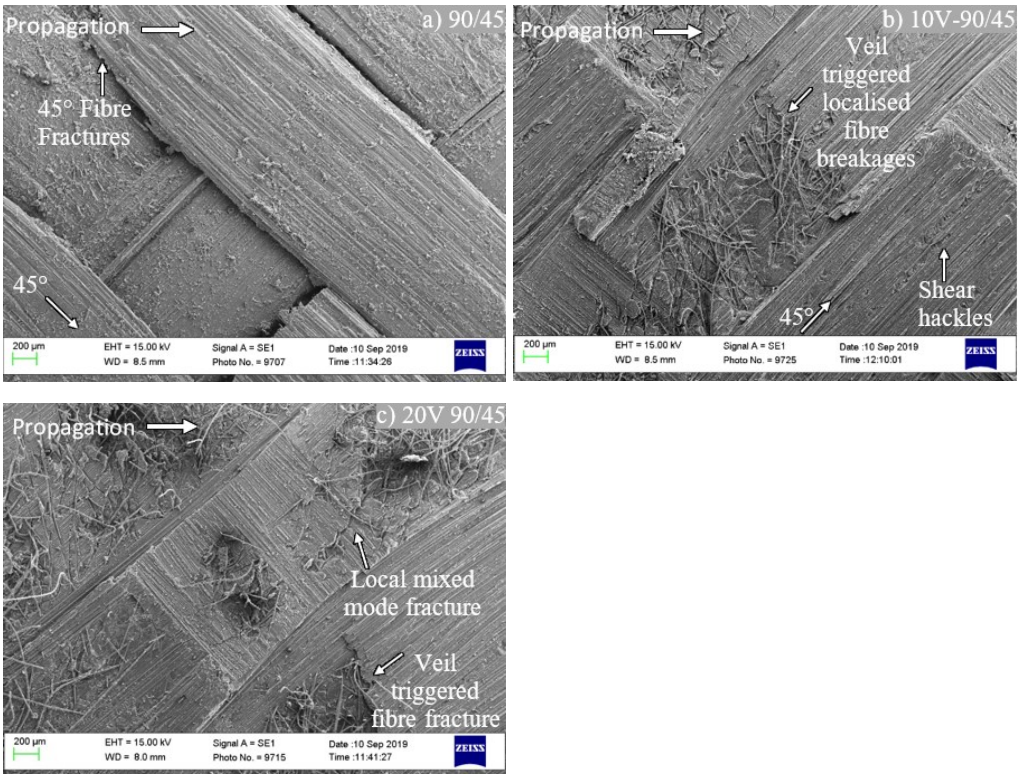

Fig.8 Fracture surface of 45° fibre orientation bias at 90/45 dominated midplane: (a) without veil, (b) 10gm^{-2} veil, and (c) 20gm^{-2} veil.

Fig.9 presents the SEM observations at the 90° fibre orientation bias fractured surface for the 90/90 dominant midplane fibre orientation. In comparison to the dominant 0/0 midplane

fibre orientation (Fig.5), specimens with dominant 90/90 midplane fibre orientations have pronounced fracture surface texture perpendicular to the delamination propagation direction. The enhanced texture transverse to the delamination path increases the resistance to the approaching delamination front compared to that of 0/0 configurations. This is closely related to the effect of interfacial fibre orientation and justifies the 72% increase in G_{IIC} for the non-interleaved 90/90 (1811J/m^2) compared with the non-interleaved 0/0 (1055J/m^2) configuration. Similar to the observation of the 0/0, interleaved 90/90 specimens (Figs.9(b-c)) exhibit coarser fracture surface than non-interleaved specimens (Fig.9(a)). The level of coarseness of interleaved 90/90 specimens presented in Fig.9 is however less severe than the interleaved 0/0 specimens (Fig.5). The resulting G_{IIC} improvements are 25% for 10v-90/90 (2255J/m^2) and 23% for 20v-90/90 (2228J/m^2) over the non-interleaved 90/90 (1811J/m^2) specimens. The combined effect of interfacial fibre orientation bias and PPS veil makes the G_{IIC} of 10v-90/90 and 20v-90/90 specimens 114% and 111% greater than non-interleaved 0/0 configurations.

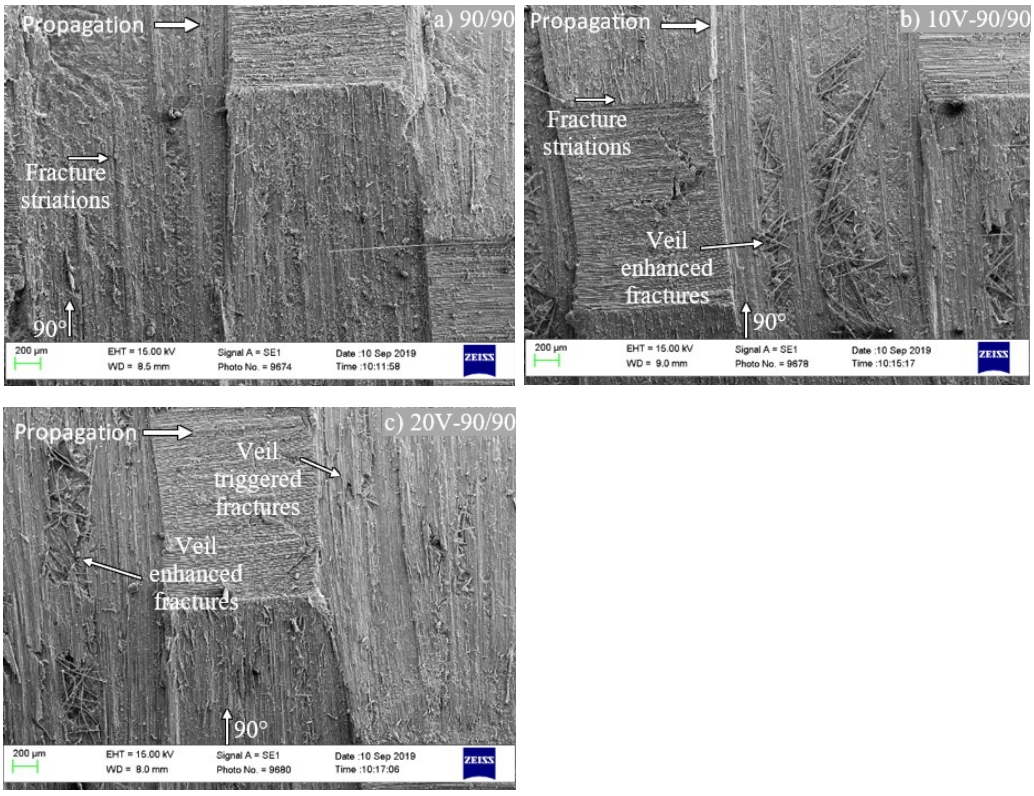

Fig.9 Fracture surface of 90° fibre orientation bias at 90/90 dominated midplane: (a) without veil, (b) 10gm^{-2} veil, and (c) 20gm^{-2} veil.

5. Discussion

The majority of studies in literature considering mode-II loading of fibre reinforced laminates interleaved with thermoplastic veils has been on unidirectional laminae, with only a limited number considering satin weaves. The limited studies involving 5HS laminae [6, 22-25] have configured the parent fibre orientation bias as predominantly 0° orientation [6,19,27,28]. The current work for the first time presents a detailed quantification considering the influence of interfacial fibre orientation bias combined with the veil density investigation on the delamination resistance under mode-II loading. Results in Table3 and Fig.4 present significant G_{IIC} variations in 5HS weave CFRP laminates with alterations in midplane interfacial fibre orientation bias and PPS veil density. Table 3 and Fig.4(a) reveal the G_{IIC} values due to the interfacial biased fibre orientation and addition of the veils being segregated into two groups; one containing the 0/0 and 0/90 interfacial biases and another group containing the 0/45, 90/45 and 90/90 biased midplane interfaces. The segregation of the two different fracture toughness groups is due to the fracture occurring either at the interface between the tough polymer and brittle matrix or within the PPS interleave. The results are rationalised with detailed fractographic analyses which identifies fibre orientation to delamination path, surface texture misfit, and veil density as the main contributors to variations of delamination resistance of 5HS woven laminates.

The fibre orientation relative to the delamination path plays a major role in the delamination resistance. The effect is twofold: the weave portions of the fibres perpendicular to the delamination path produce a step and hence a rougher fracture surface; the angled component (e.g. 45°) of the fibre orientation triggers tow-localised mixed fracture modes owing to the interfacial weave architecture. The non-interleaved 90/90 (1811J/m^2) specimens have a G_{IIC} 72% greater than the non-interleaved 0/0 (1055J/m^2) specimens. The 45° fibre orientation bias at the midplane appears to have the greatest beneficial impact on delamination resistance as it introduces both components mentioned

above. This is supported by the test results for configurations involving the 45° fibre orientation bias (0/45 and 90/45) having the greatest delamination resistance (Table 3 and Fig.4). The non-interleaved 90/45 (1921J/m^2) specimens have the largest increase (82%) than the non-interleaved 0/0 (1055J/m^2) specimens from all configurations investigated.

Surface texture misfit is another important factor affecting delamination resistance of 5HS woven laminates. The misalignment of the fibre orientation bias at the two faces of the midplane interface facilitates the formation of resin rich zones (Fig.7) which significantly reduces the delamination resistance. The non-interleaved configurations for the 0/90 fibre orientation bias have the largest surface texture misfit (90°) and the lowest G_{IIC} (1007J/m^2) of all configurations considered. The G_{IIC} of non-interleaved 0/90 (1007J/m^2) is 5% less than the non-interleaved 0/0 (1055J/m^2) specimens, suggesting the detrimental effects of resin rich zones due to surface texture misfit outweigh the toughening effect from the face of 90° fibre orientation bias perpendicular to the delamination path.

The PPS veil at the midplane improves the delamination resistance for all configurations investigated. For chopped stranded PPS interleaved veils to improve the G_{IIC}, the fibres must be tough, able to deform plastically with high elongation to break performance, have high shear strengths [29] and good adhesion to the matrix resin. The localised ductility of the interface is enhanced with chopped stranded PPS by introducing localised strain concentrations during loading, subsequently triggering the undulating fracture paths following the least resistance to fracture. Compared with non-interleaved group, interleaved configurations exhibit coarse and irregular fractographic morphologies associated with fibre bridging, breakage, fibre-matrix imprint, striations, pull-out, and shear hackles due to tow-localised mixed-mode fracture. The fracture features also demonstrate enhanced fibre-level interactions consisting of localised staggered migration tendencies [18] and diverse orientation specific fracture features. Consequently, the stronger fibre-matrix interactions introduced by the PPS veil enhances the delamination resistance. The enhancement of PPS

veil on G_{IIC} is however fibre orientation dependent with the 0/90 fibre orientation bias exhibiting the strongest beneficial effect. This can be attributed to the smoothing and cushioning effect of the veil, which has the strongest beneficial impact on specimens with the greatest surface texture misfit. The G_{IIC} of 10v-0/90 (1723J/m^2) and 20v-0/90 (1760J/m^2) are 71% and 75% higher than the non-interleaved 0/90 (1007/m^2) specimens. It is however worth noting that a further increase of the veil density from 10gm^{-2} to 20gm^{-2} offers little extra enhancement [8] to the delamination resistance as the fracture may occur within the veil interlayer. The maximum improvement in G_{IIC} when the veil density has been increased from 10gm^{-2} to 20gm^{-2} is 4% for all the configurations considered, which is very limited in contrast with the change of veil density from 0gm^{-2} to 10gm^{-2}.

Moreover, veil interleaving has been demonstrated to improve the fibre orientation sensitivity and increase the G_{IIC}, but not entirely remove the bias of the 5HS weave architecture under mode II loading. Examination of the fracture surfaces reveals the combined shear and tensile microcrack damage of the fracture surface during mode II loading occurring between the interface of the parent biased-fibre surface and the veil interleave. The representative fracture surfaces (Figs.5-9) show distinct fracture path differences between interfacial fibre orientation and the presence of the interleaved veils. It can be observed that a small quantity of delaminated and broken carbon fibres is present on the fracture surface of the non-interleaved configurations with fibres mostly attached to the fracture surface. The fracture propagation for 10gm^{-2} and 20gm^{-2} interleaved mid-planes experienced greater shear loads applied to the matrix surrounding the carbon fibres, resulting in flake-like epoxy platelet regions remaining on the fracture surfaces.

A combination of shear and tensile microcrack growth are responsible for the mode II failure of the tested configurations with a summary of key failure paths presented in Fig.10. Whilst the toughening mechanisms for veil enhancements are still not fully established, it is thought that PPS fibres bridge the microcracks within the interlayer during mode II loading.

The bridging effects absorb the fracture energy whilst the PPS fibers are well adhered to the epoxy resin matrix. Sufficient interdiffusion and enhancement of the core-shell membrane region has been previously studied [30] to consider the effect of the dispersion characteristic of nanofiber interleaves. The dispersion effect on the PPS/Epoxy may be enhanced to improve the core-shell membrane hence interfacial toughening by considering a two-step post curing process [30]. Moreover, the variation in fracture resistance is linked to the interlayer and interfacial fibre orientation. The migrating path of the fracture can increase or decrease energy depending on the proximity to longitudinal or transverse fibres. Transversely oriented fibres relative to the crack path form crack arresting features, for example, the 80% bias in the 90° dominated midplanes. Deviation from a straight path requires greater energy, hence the fracture would follow the 0° oriented tows. Under shear loading the path will follow either interfacial surface, however transversely oriented fibres will promote tow-localised migration to the weakest path shown in Fig.10 & [18].

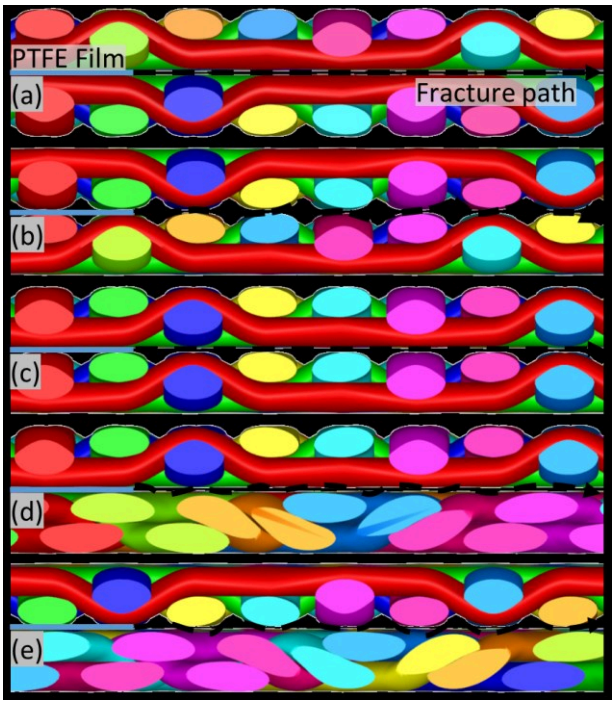

0/0 – A, F, G.
10V-0/0 – B(v), D, E, F.
20V-0/0– B(v), C, D, E, F.

90/90 – C, D, H.
10V-90/90 – B(ii), D, E, F.
20V-90/90– B(ii), D, E, F.

0/90 – A, F, G.
10V-0/90 – B(iv), C, D, E, F, H.
20V-0/90– B(v), D, E, F.

0/45 – A, D, G.
10V-0/45 – B(iv), C, D, E, H.
20V-0/45– B(v), C, D, E, F, H.

90/45 – A, D, H.
10V-90/45 – B(v), C, D, E, F, H.
20V-90/45– B(v), C, D, E, F, H.

Fig.10 Representative fracture paths and features of: (a) 0/0, (b) 90/90, (c) 0/90, (d) 0/45, (e) 90/45 biased midplanes.
Legend: Fracture surface features; ***A***=*Smooth crack propagation* / ***B***=*Bridging majority between:* ***(i)*** *0° & veil,* ***(ii)*** *90° & veil,* ***(iii)*** *45° & veil,* ***(iv)*** *Combined parent & veil,* ***(v)*** *Combined parent, matrix & veil* / ***C***=*Cusp morphology* / ***D***=*Damage - localised fibres.* ***E***=*Enhanced fibre-level interactions.* / ***F***=*Flake-like matrix remnants.* / ***G***=*Resin rich regions.* / ***H***=*Shear hackles.*

Currently, no test standard is available for the determination of G_{IIC} for multidirectional woven laminates with different veil densities. The experimental methodology adopted from D7905/D7905M – 14 [26] can lead to inconsistencies in the output when applied to 5HS laminates owing to the warp and weft surface irregularities of the fabric reinforcement. This work aims to highlight the necessity for developing a standardized approach when dealing with satin weave architectures and interleaving. Discrepancies and calculation limitations can arise when using the experimental methodology intended for UD toughness calculations for alternative layups, including issues with stress fluctuation, crack re-nucleation, bifurcation [29], fracture migration [18,31,32] and coupling between tension and bending for unsymmetrical laminates which could alter the specimen neutral axis. Current engineering design and analysis approaches commonly disregard crucial aspects including layup related fibre-matrix interaction, tow-localised mixed-mode fracture tendencies, migration, and density of interleaving. Test standard D7905/D7905M – 14 [26], measuring the G_{IIC} of UD laminate at the 0/0 interface, is inadequate to evaluate the structural performance of multidirectional woven laminates due to the findings that G_{IIC} are strongly dependent on the interfacial fibre orientation and veil density. It can be observed in Table3 and Fig.4 that the G_{IIC} for 0/0 interfacial fibre orientation biases are in general much lower than other interfacial fibre orientation biases. The fracture toughness values obtained from the current multidirectional 3ENF tests are valid for the design and analysis of 5HS laminated structures of the same layup configurations. The need to develop woven fabric specific test standards is apparent, to better characterise the fracture mechanisms and structural performance of multidirectional woven laminates with toughening interlayers. The knowledge developed from valid test standards can aid in achieving better design flexibility and reliability, and has direct industrial relevance to the optimised damage tolerance design and modelling strategy for laminated woven composite structures.

6. Conclusions

The following conclusions can be drawn from the 3ENF tests and fractographic analysis for the effects of interfacial fibre orientation and interleaved thermoplastic veil on delamination resistance of 5HS woven laminates under mode II loading:

- Fibre orientation relative to the delamination path, surface texture misfit, and veil density are the three main factors affecting delamination resistance at the midplane of 5HS woven laminates.
- Fibres oriented at an angle to the overall delamination path introduces a torturous fracture path with rougher fracture surfaces and tow-localised mixed mode fracture tendencies, hence improve delamination resistance compared with fibres parallel to the delamination path. Configurations containing the 90/45 interfacial fibre orientation bias have the greatest G_{IIC} of all the layup configurations considered.
- The misalignment of the fibre orientation due to surface texture misfit at the midplane facilitates the formation of resin rich zones which can significantly reduce the delamination resistance. The addition of thermoplastic veil can effectively reduce the detrimental effect of resin rich zones stemming from surface texture misfits.
- Thermoplastic veil at the midplane strengthens fibre-matrix interactions and improves the delamination resistance for all layup configurations investigated. The enhancement is however fibre orientation dependent with 0/90 fibre orientation biases exhibiting the strongest beneficial effect. A further increase of the veil density from $10gm^{-2}$ to $20gm^{-2}$, however, offers little extra enhancement to the delamination resistance.
- Test standards suitable for G_{IIC} measurement of woven laminates are highly desirable to the optimised damage tolerance design and modelling strategy for laminated woven composite structures.

Acknowledgements

The authors would like to thank Technical Fibre Products for supplying the Optiveil PPS veils used for this investigation. The authors would also like to thank Jarryd Braithwaite for laboratory assistance during testing at Cranfield University and Richard Giddens for SEM support at Kingston University. Amit Ramji would like to acknowledge SATM at Cranfield University for funding this research.

References

[1] M. Grasso, Y. Xu, A. Ramji, G. Zhou, A. Chrysanthou, G. Haritos, Y. Chen, Low-velocity impact behaviour of woven laminate plates with fire retardant resin, Compos. Part B Eng. 171 (2019) 1–8. https://doi.org/10.1016/j.compositesb.2019.04.023.

[2] X. Tang, J.D. Whitcomb, Progressive Failure Behaviours of 2D Woven Composites, J. Compos. Mater. 37 (2003) 1239–1259. https://doi.org/10.1177/002199803033468.

[3] N.H. Nash, T.M. Young, W.F. Stanley, An investigation of the damage tolerance of carbon/Benzoxazine composites with a thermoplastic toughening interlayer, Compos. Struct. 147 (2016) 25–32. https://doi.org/10.1016/j.compstruct.2016.03.015.

[4] V.A. Ramirez, P.J. Hogg, W.W. Sampson, The influence of the nonwoven veil architectures on interlaminar fracture toughness of interleaved composites, Compos. Sci. Technol. 110 (2015) 103–110. https://doi.org/10.1016/j.compscitech.2015.01.016.

[5] R. Palazzetti, A. Zucchelli, Electrospun nanofibers as reinforcement for composite laminates materials – A review, Compos. Struct. 182 (2017) 711–727. https://doi.org/10.1016/j.compstruct.2017.09.021.

[6] P.J. Hogg, Toughening of thermosetting composites with thermoplastic fibres, Mater. Sci. Eng. A. 412 (2005) 97–103. https://doi.org/10.1016/j.msea.2005.08.028.

[7] L. Daelemans, S. van der Heijden, I. De Baere, H. Rahier, W. Van Paepegem, K. De Clerck, Nanofibre bridging as a toughening mechanism in carbon/epoxy composite laminates interleaved with electrospun polyamide nanofibrous veils, Compos. Sci. Technol. 117 (2015) 244–256. https://doi.org/10.1016/j.compscitech.2015.06.021.

[8] G.W. Beckermann, K.L. Pickering, Mode i and Mode II interlaminar fracture toughness of composite laminates interleaved with electrospun nanofibre veils, Compos. Part A Appl. Sci. Manuf. 72 (2015) 11–21. https://doi.org/10.1016/j.compositesa.2015.01.028.

[9] M.W. Czabaj, J.G. Ratcliffe, Comparison of intralaminar and interlaminar mode-I fracture toughness of unidirectional IM7/8552 graphite/epoxy composite, NASA Tech. Rep. (2012) 1–18. https://doi.org/10.1016/j.compscitech.2013.09.008.

[10] M. Yasaee, I.P. Bond, R.S. Trask, E.S. Greenhalgh, Damage control using discrete thermoplastic film inserts, Compos. Part A Appl. Sci. Manuf. 43 (2012) 978–989. https://doi.org/10.1016/j.compositesa.2012.01.011.

[11] M. Yasaee, I.P. Bond, R.S. Trask, E.S. Greenhalgh, Mode I interfacial toughening through discontinuous interleaves for damage suppression and control, Compos. Part

A Appl. Sci. Manuf. 43 (2012) 198–207. https://doi.org/10.1016/j.compositesa.2011.09.026.

[12] J.W. Kim, J.S. Lee, Influence of interleaved films on the mechanical properties of carbon fiber fabric/polypropylene thermoplastic composites, Mater. MDPI. 9 (2016) 1–12. https://doi.org/10.3390/ma9050344.

[13] F. Bovicelli, H. Saghafi, T.M. Brugo, J. Belcari, a. Zucchelli, G. Minak, On Consideration the Mode I Fracture Response of CFRP Composite Interleaved by Composite Nanofibers, Procedia Mater. Sci. 3 (2014) 1316–1321. https://doi.org/10.1016/j.mspro.2014.06.213.

[14] N.H. Nash, T.M. Young, W.F. Stanley, The influence of a thermoplastic toughening interlayer and hydrothermal conditioning on the Mode-II interlaminar fracture toughness of Carbon/Benzoxazine composites, Compos. Part A Appl. Sci. Manuf. 81 (2016) 111–120. https://doi.org/10.1016/j.compositesa.2015.11.010.

[15] C. Cheng, Z. Chen, Z. Huang, C. Zhang, R. Tusiime, J. Zhou, Z. Sun, Y. Liu, M. Yu, H. Zhang, Simultaneously improving mode I and mode II fracture toughness of the carbon fiber/epoxy composite laminates via interleaved with uniformly aligned PES fiber webs, Compos. Part A Appl. Sci. Manuf. 129 (2020) 1–11. https://doi.org/10.1016/j.compositesa.2019.105696.

[16] L. Daelemans, S. van der Heijden, I. De Baere, H. Rahier, W. Van Paepegem, K. De Clerck, Using aligned nanofibres for identifying the toughening micromechanisms in nanofibre interleaved laminates, Compos. Sci. Technol. 124 (2016) 17–26. https://doi.org/10.1016/j.compscitech.2015.11.021.

[17] M. Yasaee, G. Mohamed, A. Pellegrino, N. Petrinic, S.R. Hallett, Strain rate dependence of mode II delamination resistance in through thickness reinforced laminated composites, Int. J. Impact Eng. 107 (2017) 1–11. https://doi.org/10.1016/j.ijimpeng.2017.05.003.

[18] A. Ramji, Y. Xu, M. Yasaee, M. Grasso, P. Webb, Delamination migration in CFRP laminates under mode I loading, Compos. Sci. Technol. 190 (2020) p1-10. https://doi.org/10.1016/j.compscitech.2020.108067.

[19] D. Quan, F. Bologna, G. Scarselli, A. Ivanković, N. Murphy, Mode-II fracture behaviour of aerospace-grade carbon fibre/epoxy composites interleaved with thermoplastic veils, Compos. Sci. Technol. 191 (2020) 1–10. https://doi.org/10.1016/j.compscitech.2020.108065.

[20] N. V De Carvalho, B.Y. Chen, S.T. Pinho, J.G. Ratcliffe, P.M. Baiz, T.E. Tay, Modeling delamination migration in cross-ply tape laminates, Compos. Part A Appl. Sci. Manuf. 71 (2015) 192–203. https://doi.org/10.1016/j.compositesa.2015.01.021.

[21] L. Banks-Sills, C. Ishbir, V. Fourman, L. Rogel, R. Eliasi, Interface fracture toughness of a multi-directional woven composite, Int. J. Fract. 182 (2013) 187–207. https://doi.org/10.1007/s10704-013-9868-6.

[22] A.F. Gill, P. Robinson, S. Pinho, Effect of variation in fibre volume fraction on modes I and II delamination behaviour of 5HS woven composites manufactured by RTM, Compos. Sci. Technol. 69 (2009) 2368–2375. https://doi.org/10.1016/j.compscitech.2009.02.008.

[23] S.G. Ivanov, D. Beyens, L. Gorbatikh, S. V. Lomov, Damage development in woven carbon fibre thermoplastic laminates with PPS and PEEK matrices: A comparative study, J. Compos. Mater. 51 (2016) 637–647. https://doi.org/10.1177/0021998316653460.

[24] Cytec Industrial Materials, MTM 49-3 Data Sheet, PDS1258_07.13. (2012) 1–4. https://cytec.com/sites/default/files/datasheets/MTM49.pdf (accessed May 2, 2019).

[25] TFP, Opti veil ® OP-49-48-PPS Technical Datasheet, (2015) 1–2. http://www.tfpglobal.com/materials/thermoplastic/OP-49-48-PPS (accessed May 2, 2019).

[26] ASTM-D7905/D7905M-14, Standard Test Method for Determination of the Mode II Interlaminar Fracture Toughness of Unidirectional Fiber-Reinforced Polymer Matrix Composites, Am. Soc. Test. Mater. 15.03 (2014) 1–18.

[27] D. Quan, R. Alderliesten, C. Dransfeld, N. Murphy, A. Ivanković, R. Benedictus, Enhancing the fracture toughness of carbon fibre/epoxy composites by interleaving hybrid meltable/non-meltable thermoplastic veils, Compos. Struct. 252 (2020). https://doi.org/10.1016/j.compstruct.2020.112699.

[28] D. Quan, B. Deegan, R. Alderliesten, C. Dransfeld, N. Murphy, A. Ivanković, R. Benedictus, The influence of interlayer/epoxy adhesion on the mode-I and mode-II fracture response of carbon fibre/epoxy composites interleaved with thermoplastic veils, Mater. Des. 192 (2020) 1–10. https://doi.org/10.1016/j.matdes.2020.108781.

[29] X. Ni, C. Furtado, N.K. Fritz, R. Kopp, P.P. Camanho, B.L. Wardle, Interlaminar to intralaminar mode I and II crack bifurcation due to aligned carbon nanotube reinforcement of aerospace-grade advanced composites, Compos. Sci. Technol. 190 (2020) 108014. https://doi.org/10.1016/j.compscitech.2020.108014.

[30] L. Daelemans, N. Kizildag, W. Van Paepegem, D.R. D'hooge, K. De Clerck, Interdiffusing core-shell nanofiber interleaved composites for excellent Mode I and Mode II delamination resistance, Compos. Sci. Technol. 175 (2019) 143–150. https://doi.org/10.1016/j.compscitech.2019.03.019.

[31] C.J. Hsueh, L. Avellar, B. Bourdin, G. Ravichandran, K. Bhattacharya, Stress fluctuation, crack renucleation and toughening in layered materials, J. Mech. Phys. Solids. 120 (2018) 68–78. https://doi.org/10.1016/j.jmps.2018.04.011.

[32] Y. Gong, B. Zhang, S.R. Hallett, Delamination migration in multidirectional composite laminates under mode I quasi-static and fatigue loading, Compos. Struct. 189 (2018) 160–176. https://doi.org/10.1016/j.compstruct.2018.01.074.

Appendix A

Table A-1 Data for 90/90 Bias

Steel Calibration Bar (Width 40.2 x Thick 15.24mm), Cs= Slope (dLoad/dDisp)= 0.093836									
	90/90			10v-90/90			20v-90/90		
	C/Cs			C/Cs			C/Cs		
Specimen run #	1	2	3	1	2	3	1	2	3
NPCa1 (a=20mm)	2.8%	1.7%	2.6%	1.8%	2.7%	2.9%	1.9%	2.6%	3.0%
NPCa2 (a=40mm)	1.7%	1.0%	1.5%	1.1%	1.7%	1.7%	1.1%	1.6%	1.8%
NPCa0 (a=30mm)	2.3%	1.3%	2.1%	1.4%	2.3%	2.3%	1.5%	2.2%	2.4%
PCa1 (a=10mm)	2.7%	1.7%	2.7%	1.8%	2.9%	2.9%	2.0%	2.7%	3.1%
PCa2 (a=40mm)	1.8%	1.1%	1.7%	1.2%	2.0%	1.9%	1.2%	1.9%	2.1%
PCa0 (a=30mm)	2.3%	1.4%	2.3%	1.6%	2.6%	2.4%	1.6%	2.5%	2.7%
Max $P_{a0\ (NPC)}$ [N]	588	428	557	512	606	611	518	564	588
Max $P_{a0\ (PC)}$ [N]	966	688	877	910	1163	1002	897	1175	1100
G_{IIC_NPC} [J/m^2] (Eqn.1-3)	***880.9**	811	996	950	832	1011	916	874	907
G_{IIC_PC} [J/m^2] (Eqn.1-3)	***1999.8**	1742	1832	2342	2492	2256	2331	2400	2394
Avg_G_{IIC_NPC} [J/m^2]	896			931			899		
Avg_G_{IIC_PC} [J/m^2]	1858			2364			2375		

Table A-2 Sample Mode II Fracture Toughness Calculation

Steel Calibration Bar (Width 40.2 x Thick 15.24mm), Cs= Slope (dLoad/dDisp)= 0.093836				
Layup	G_{II}-1-C9090-1			
Ply Thickness, t (mm)	0.32			
Thickness, t (mm)	4.52			
Width, B (mm)	20.25			
	Crack length (a) [mm]	Crack length (a^3) [mm^3]	(Eqn.1) C=A+ma^3 [mm/kN]	Cs/C
NPCa1	20	8000	3.4019	2.8%
NPCa2	40	64000	5.5293	1.7%
NPCa0	30	27000	4.0617	2.3%
PCa1	20	8000	3.4733	2.7%
PCa2	40	64000	5.2579	1.8%
PCa0	30	27000	4.0036	2.3%
m_{NPC}=SLOPE(δC, δa^3)$_{NPC}$	3.822E-05			
m_{PC} =SLOPE(δC, δa^3)$_{PC}$	3.215E-05			
Max $P_{a0\ (NPC)}$ [N]	588.0			
Max $P_{a0\ (PC)}$ [N]	966.0			
(Eqn.3) G_{IIC} =$(3mP^2\ a^2)/2B$				
G_{IIC_NPC} [J/m^2]	=(3*m_{NPC}*(588^2)*(30^2))/(2*20.25) = **880.9**			
G_{IIC_PC} [J/m^2]	=(3*m_{PC}*(966^2)*(30^2))/(2*20.25) = **1999.8**			